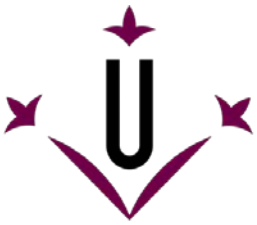

Energetic simulation of a dielectric photovoltaic-thermal concentrator

A. Moreno[1], A. Riverola[1], D. Chemisana[1,*]

[1]Applied Physics Section of the Environmental Science Dept., University of Lleida, 25001 Lleida, Spain.

Abstract

A solar concentrating photovoltaic-thermal (CPVT) module with cell immersion in dielectric liquid has been modeled and energetically simulated. The concentrator focuses radiation linearly by using a cylindrical shape optics made of polymethyl methacrylate. The geometric concentration is 12 suns with an optical efficiency of 76.14%. The dielectric fluid, deionized water, flows through the concentrator case fulfilling a double function: to concentrate and to cool the PV cells. The concentrator is designed to be superimposed in front of the windows in a 2-storey family house with 4-person occupancy. The system is modeled to partially cover thermal and electrical demands utilizing a radiant floor and a reversible air-air heat pump for space heating and cooling (SH&C) and an electrical circuit which combines direct consumption and battery storage. The system topology has been simulated for three locations (Lisbon, Barcelona and Genoa). Results indicate an appropriate performance of the system analyzed with DHW solar fractions in a range from around 61% to above 75%. The lowest corresponds to Genoa and the highest to Lisbon and Barcelona. Regarding SH&C solar fractions are also quite adequate with values ranging from 38.3 % (Genoa) to above 60% (68.8 % in Lisbon and 62.4% in Barcelona). Finally, SFs for electrical loads take a value of 44.09% in the case of Lisbon, 38.9% for Barcelona and 23.51% for Genoa.

1. Introduction

Reducing energy consumption in the building sector is of ongoing concern. In the European Union, this sector accounts for 40% of the total energy consumption. As a consequence, the European Commission developed the energy performance building directive (EPBD) which states the “20-20-20” objectives: reduction of 20% in greenhouse-gas emissions, a share of renewable energy of 20% and an improvement of 20% in energy efficiency [1]. A feasible solution to address the EPBD objectives is the building integration of hybrid photovoltaic-thermal (PVT) solar collectors. PVT systems can be a high-efficient technology able to cogenerate heat and electricity with global efficiencies around 70%, with electrical efficiencies near 20% and thermal efficiencies higher than 50% [2]. Moreover, building integrated PVT devices have demonstrated to be more efficient than separated conventional solar energy systems, which would need 60% additional area to produce the same amount of energy [3]. Although PV and PVT prices tend to decrease, the cost of PVT systems and its environmental impact still limit a wider application of this technology. One efficient strategy, which reduces both the cost and the environmental impact while increasing the efficiency, is to reduce the cell size by

concentrating incident light into a smaller area, the so-called concentrating photovoltaic-thermal (CPVT) systems [4,5]. In the case of CPVT devices, temperature management becomes an important issue since the energy flux received by the cell grows proportionally to the concentration ratio and the biggest part of it is converted into heat.

On the other hand, CPVT systems based on direct immersion of PV cells in dielectric liquids can achieve an additional efficiency enhancement with respect to standard CPVTs. Some of the most important aspects leading to this efficiency enhancement rely on: (1) a reduction of the Fresnel losses and surface recombination with respect to a bare cell [7] and (2) a better PV temperature control since the contact thermal resistance between the cell and the cooling system tends to decrease or even almost disappear and the heat is extracted on the cell front and rear surfaces, whereas in conventional systems only the rear surface is in contact [8]. Also, it should be noted that the liquids selected absorb photons not contributing to electrical generation before reaching the cell, preventing from possible overheating cell effects [9].

Despite these notable benefits described above, very few direct immersed CPVTs studies can be found in the literature [10–13] and specifically, to the best of the authors' knowledge, no research regarding building integrated direct immersed CPVTs has been conducted yet. It should be noted that in the case of non-concentrating direct immersed PVTs for building applications further investigation is also needed [9].

In order fill the gap in the literature about direct immersed PVTs, especially CPVTs, for building applications and taking into account the potential of these collectors regarding the on-site cogeneration, it can be seen that there is a need for investigating them. In the frame of this concept, the dynamic energy performance of a building façade integrated CPVT collector is studied to determine its feasibility in covering the energy demands of a typical 2-story single-family house for three different locations: Lisbon (Portugal), Barcelona (Spain) and Genoa (Italy).

The present research is structured in three main sections. First of all, the CPVT module developed and the building where it is superimposed are described. Afterwards, the methodology followed up in the modeling is explained. Finally, the results obtained are presented and the main conclusions are stated.

2. Module and building description

2.1 Module description

The CPVT system is designed to be superimposed on the south-facing windows of a typical residential or offices building. The concentrator is composed of a cylindrical shape polymethyl methacrylate (PMMA) chassis and a dielectric liquid where the PV cells are immersed. The geometry of the cavity filled with the dielectric fluid (deionized water, DIW) has been designed to focus irradiance towards the cell maximizing PV cell efficiency (optical efficiency and uniformity) and minimizing chromatic aberration. The aperture area of the individual modules is 80 cm long by 6 cm wide. Figure 1 sketches an isometric and cross-sectional view of a module. It can be appreciated the shape of the cavity where the DIW circulates. The interface PMMA-DIW has been designed based on a freeform profile optimization whose merit function is maximized to meet the desired

requirements (optical efficiency, uniformity and chromatic aberration). The main optical parameters are summed up in Table 1, where C_g is the geometric concentration ratio (quotient between aperture area and PV cells area), η_o is the optical efficiency (relation between the power reaching the PVs and the incident power) and α is the uniformity parameter, (quotient between the maximum difference of local irradiances at the receiver plane and the sum of the maximum and minimum local irradiances). The full optical design and methodology will be described in detail in a specific manuscript.

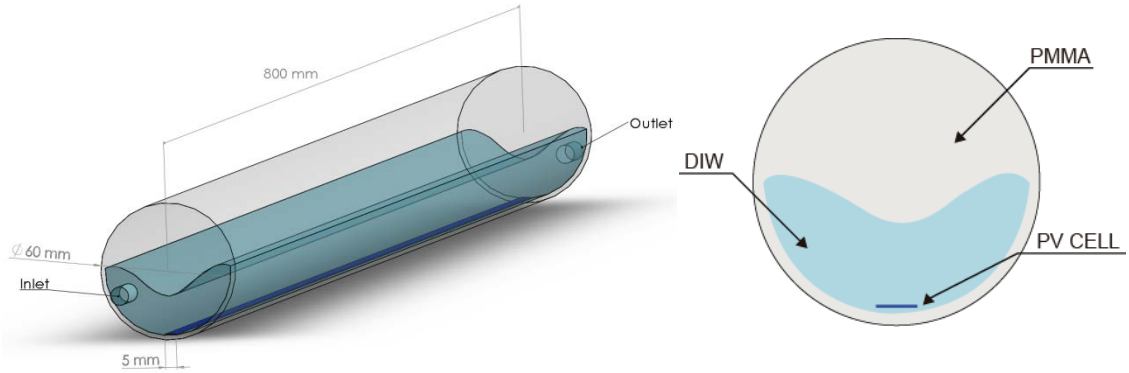

Figure 1. Schematic of a module: isometric (left) and cross-sectional (right) views.

Table 1. Optical characteristics of the system

C_g (-)	η_o (%)	α (-)
12x	76.14	0.05

Every CPVT module comprises 6 cells connected in series of 12 cm long by 0.5 cm wide each. The photovoltaic cells utilized are commercial passivated emitter rear cells (PERCs) by SAS [14] adapted to the required geometry by laser cutting, whose main electrical characteristics are shown in Table 2. V_{oc} is the open-circuit potential, J_{sc} is the short-circuit density current, FF is the fill factor, η_e is the mean electrical efficiency of the cells and γ is the power temperature coefficient.

Table 2. Parameters of the PV cells [14].

V_{OC}(V)	Jsc (mA/cm^2)	FF (%)	η_e(%)	γ (%/°C)
0.662	40.11	79.85	21.1	-0.375

The modules have been thermally characterized by a computational fluid dynamic (CFD) model conducted in COMSOL Multiphysics and by experimental assessment. The exact 3D geometry depicted in Figure 1 was drawn and meshed, ensuring the results are mesh-independent.

The COMSOL model has been initially validated by comparing theoretical results with experimental measurements performed under controlled laboratory conditions. The case consisted in characterizing the module as a dissipater. The module was completely

isolated with a 40 cm rock wool layer approaching well adiabatic exterior conditions. The heat flux exiting the cells was replicated by connecting the PVs to a power source and operating as passive electronic component dissipating power by Joule effect. The principal parameters that were monitored are: Inlet, outlet and cell temperatures jointly with flow rate. The boundary conditions of the CFD model were adapted to the experimental set-up and can be seen in Table 3.

Table 3. Description of principal boundary conditions used in CFD model.

Description	**CFD boundary cond.**	**Values**
Outer surface of the module	Adiabatic wall (a)	
Liquid cavity perimeter	No-slip (b)	
Heat generated by the PVs	Surface heat flux (c)	3007 W/m^2
Liquid inlet	Inlet flow rate (d) at certain temperature (e)	0.0018 kg/s [25-27.5]ºC

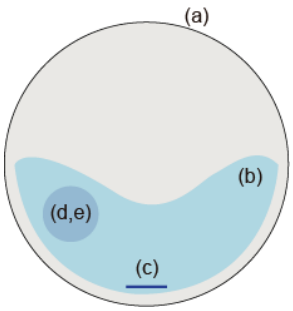

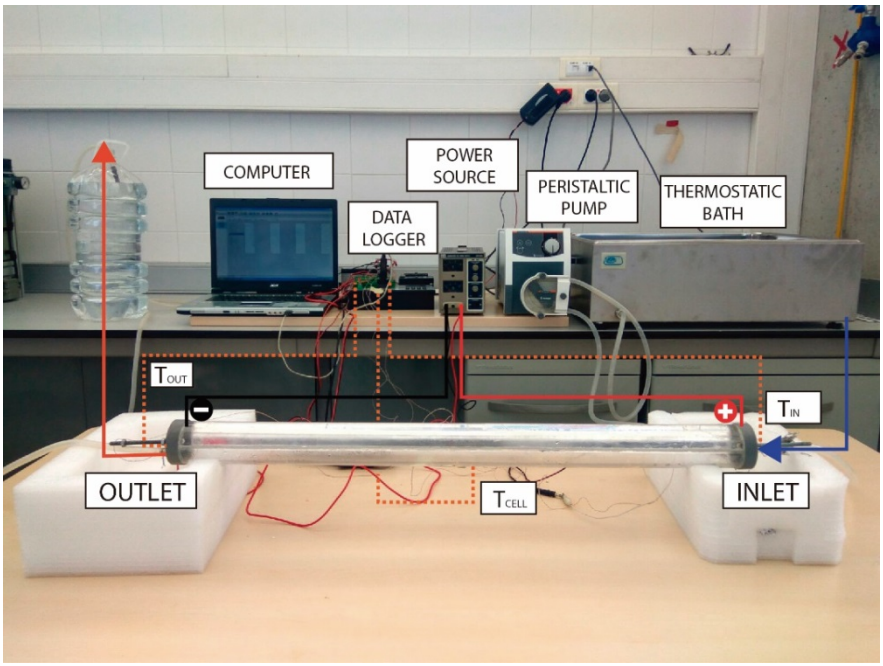

Figure 2. Scheme of the experimental setup principal elements.

Looking at Figure 2, the experimental set-up can be seen. Four different inlet temperatures, controlled with a thermostatic bath, have been assessed. These temperatures have been fixed until the collector outlet temperature was kept constant in order to obtain steady-state values. Transient and steady-state simulations reproducing the experimental conditions stablished were performed for wider validation, not only regarding stationary

values but also in the outlet temperature temporal evolution at the beginning of the experiment when all the module components (optics, PVs and liquid) were at the same temperature. Both results are depicted in Figure 3 (a) and (b). In addition, a temperature contour image from COMSOL is plotted in Figure 2 (c), illustrating, at the longitudinal central section, the spatial evolution of the temperature in the module. The PV cells are situated at the bottom (considered as volumetric heat source) delivering heat towards the coolant liquid. An excellent agreement has been achieved between modeled and experimental results with relative errors in the transient validation lower than 2% and a correlation coefficient for the steady-state numerical and experimental values of practically 1.

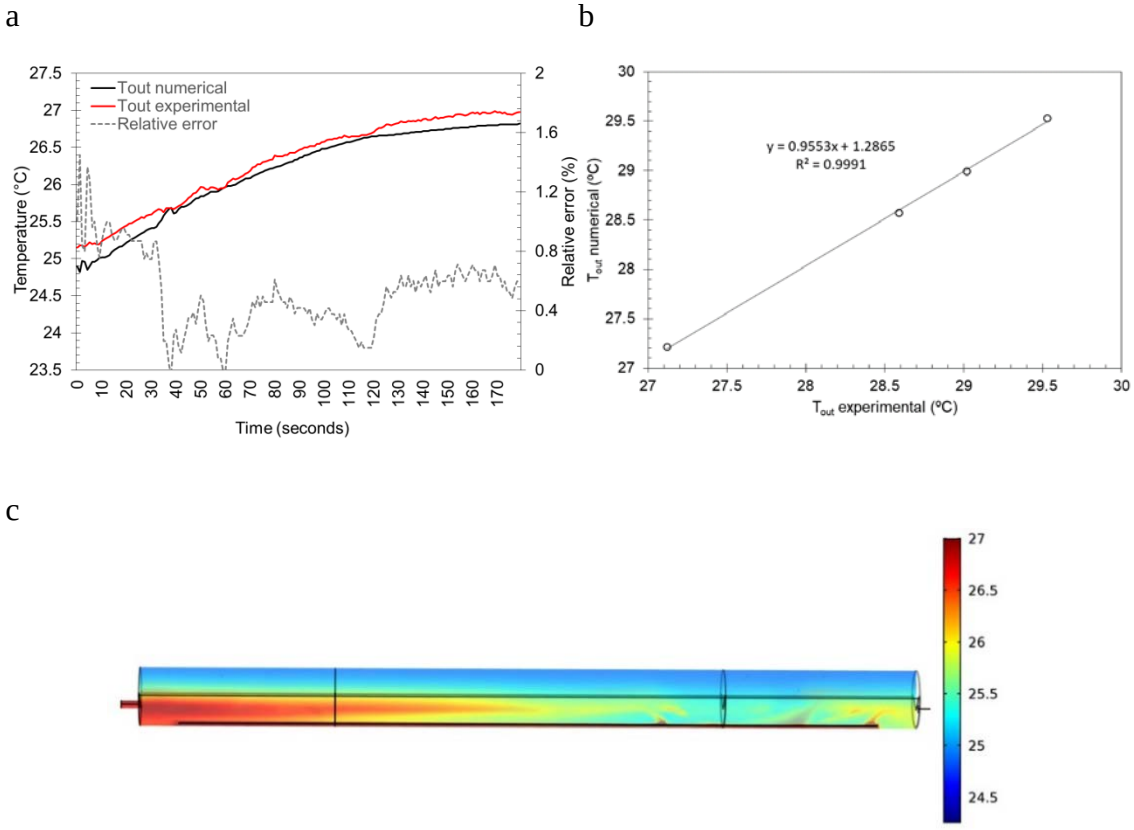

Figure 3. (a) Transient validation; (b) Steady-state validation with 4 inlet and outlet temperatures and (c) Temperature contour from the CFD simulation in COMSOL (temperatures in ºC).

Once the model was validated, the collector thermal characteristic curve has been calculated by varying inlet temperatures and irradiances. In addition, a set of thermal characteristic curves have been obtained for different wind speeds conducting a parametric study. The parametric study results in determining the wind speed dependences of the zero loss and the heat losses terms of the characteristic curve. Wind speed variations have been approached by means of convection heat transfer coefficients, calculated using Churchill and Bernstein correlation [15]. The obtained thermal characteristic curve will be later incorporated in the dynamic energetic simulation to model the thermal performance of the CPVT module.

Moreover, the collector was experimentally characterized operating under real conditions with the PV cells connected to a maximum power point tracker. The experimental outdoor measurements were carried out at the Applied Energy Research Centre (CREA) of the University of Lleida (in Spain) which is located in Lleida, at latitude 41.36°N and longitude 0.37°E. The module was placed on a two-axis tracker to ensure stable incident irradiance. The steady-state thermal characteristic curve was then obtained by varying the inlet temperature with a thermostatic bath. The inlet and outlet fluid and ambient temperatures, wind speed and solar radiation data were measured using type-T thermocouples, a Vector A-100R cup anemometer and a Kipp & Zonen CMP6, respectively. The steady-state thermal characteristic curve was compared to a simulation with analogous boundary conditions to those of the experiment.

The numerical and experimental stationary characteristic curves are shown in Figure 4.As it can be appreciated, the heat losses coefficients obtained are high, around 13-14 W/ºCm^2. This is attributed to two factors: the first is that the wind velocity of the experiment and the simulation was 2 m/s and the second is due to the morphology of the collector, in which the glazing is optimized for concentrating the incident irradiance but not for minimizing the heat losses. Good agreement is obtained between experimental and numerical values. Minor discrepancies are mainly attributed to fluctuating wind speed during the steady-state experiments around 2 m/s.

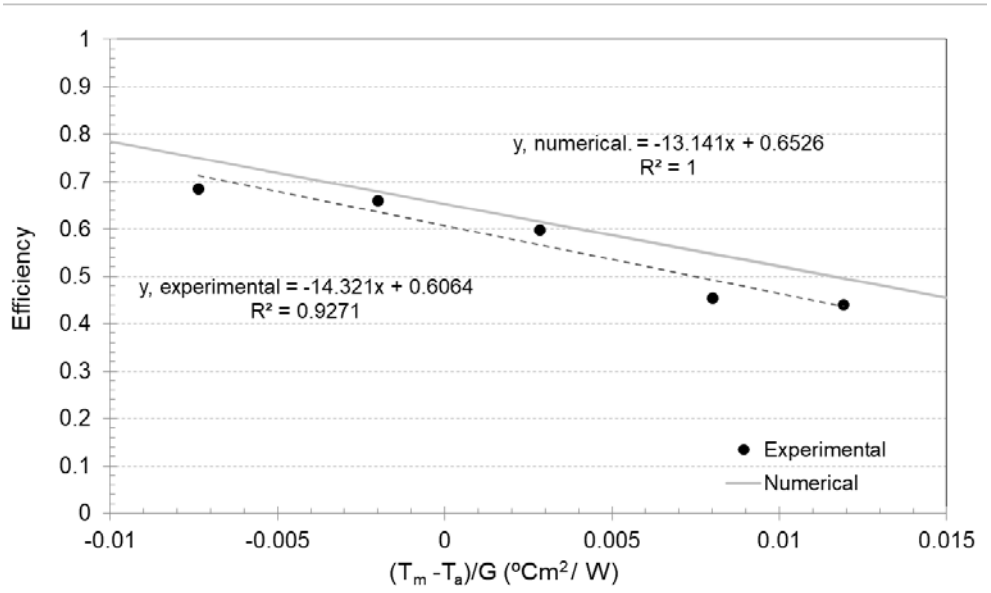

Figure 4. Thermal characteristic curve under wind velocity of 2 m/s. T_m refers to the mean fluid temperature.

The modules are designed to be placed in rows so that the appearance is similar to ordinary blinds. In the same way, it acts as shading element, which allows controlling the amount of light entering inside the building.

The concentrator has solar altitude tracking, which is achieved by rotating simultaneously all the modules in order the aperture plane to face the sun. In addition, a second movement has been implemented to control the vertical distance between modules to ensure no shading between them. Although there is a distance between modules that optimizes energy production, this second movement also allows controlling the lighting depending on the user's requirements to prioritize lighting against thermal and electrical generation.

2.2 Building description

The selected building to perform the dynamic simulation with the CPVT incorporated is a 2-story single-family house with two differentiated thermal zones associated to each floor. The building main parameters are summarized in Table 4.

The CPVT system has been integrated in front of the south-facing windows as depicted in Figure 5. Every row of collectors is composed of 4 CPVT series connected modules covering all the window width (3.2 m). There are 21 rows per window. Since each module has an aperture width of 6 cm, the system covers almost the total window height (1.3 m) when the distance between modules is set to zero. The maximum attainable occupation, and thus the interspace between collector rows, is limited by the distance between windows. For the present case, the maximum interspace is fixed to 140 mm. which ensures no shading effects till 68 º incident angle. This value has been selected as a compromise between the usable building façade, the shading losses and the effective collection area of the module.

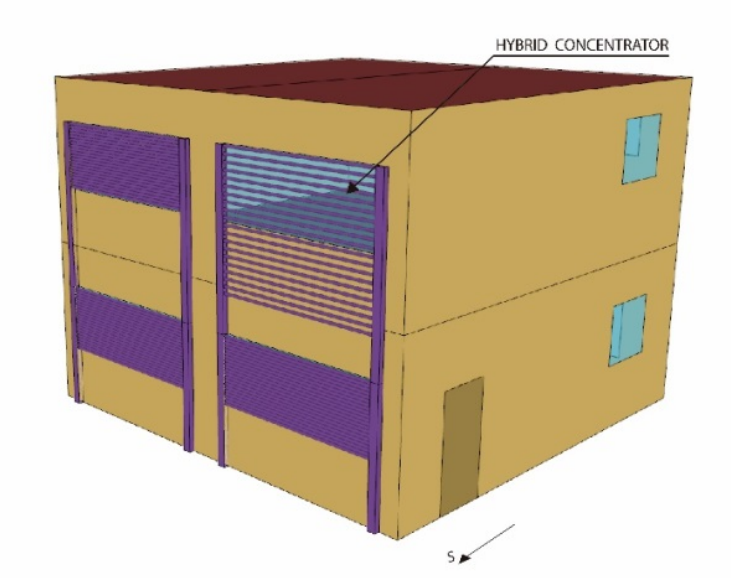

Figure 5. Architectural image of the building. At the top-right window a detail of the modules with maximum interspace is included.

Table 4. Building parameters

Parameter	Description	Value	Units
$A_{building}$	Habitable area	144.5	m^2
N_{floor}	Number of floors (zones)	2	
$H_{building}$	Building height	6	m
H_{floor}	Floor height	2.5	m
A_{face}	Area of south, north, east and west faces	54.4	m^2
$G_{southface}$	Glazed area of south face	16.5	m^2
$G_{eastface}$	Glazed area of east face	2.8	m^2
$G_{westface}$	Glazed area of west face	2.8	m^2
$G_{northface}$	Glazed area of north face	10.9	m^2

3. Methodology

The energetic simulation has been conducted in TRNSYS16 software [16] where the building is defined jointly with its system components. In the following paragraphs, first the three selected locations are presented, then the demands associated to the building are shown and finally the topology and TRNSYS model are explained.

3.1 Selected locations

The CPVT system performance has been assessed in three different locations Lisbon (Portugal, Latitude: 38.7º, Longitude: -9.14º), Barcelona (Spain, Latitude: 41.4º, Longitude: 2.15º), and Genoa (Italy, Latitude: 44.4º, Longitude: 8.94º). These cities are representative of the Csa climate ("C"-Warm, "s"-summer dry and "a"-hot summer) of the Köppen-Geiger climate classification [17]. The three locations have been selected attending to tracking and thermal performance limitations of the CPVT system. From the tracking point of view, low latitudes mean high solar altitude values and in consequence very big interspace between submodules would be necessary to prevent from shading. Also, this fact would worsen the space occupation effectiveness. On the other hand, in configurations similar to the present system, in which the interspace between modules is limited and therefore the maximum solar altitude attainable without shading, the system would experience important shading between modules considerably during summer months. Regarding high latitudes, the restriction comes from the thermal performance of the collector whose heat losses coefficient indicates a not good performance for locations with big difference between ambient and fluid temperatures.

In this study, typical meteorological year weather data from the Meteonorm TRNSYS database has been used. This data is hourly based and represents long-term statistical trends and patterns.

Figure 6 shows the monthly cumulated global horizontal irradiance (GHI) and the average ambient temperatures for the three selected locations. Lisbon has the highest annual cumulated GHI (1683 kWh/m^2), closely followed by Barcelona with 1536 kWh/m^2. Genoa presents a lower value of 1257 kWh/m^2. The monthly data depicted in the graph illustrates a similar trend with Lisbon receiving higher irradiances followed by Barcelona and Genoa. The annual average temperatures are 16.8 °C in Lisbon, 15.3 °C in Barcelona and 15.7 ºC in Genoa.

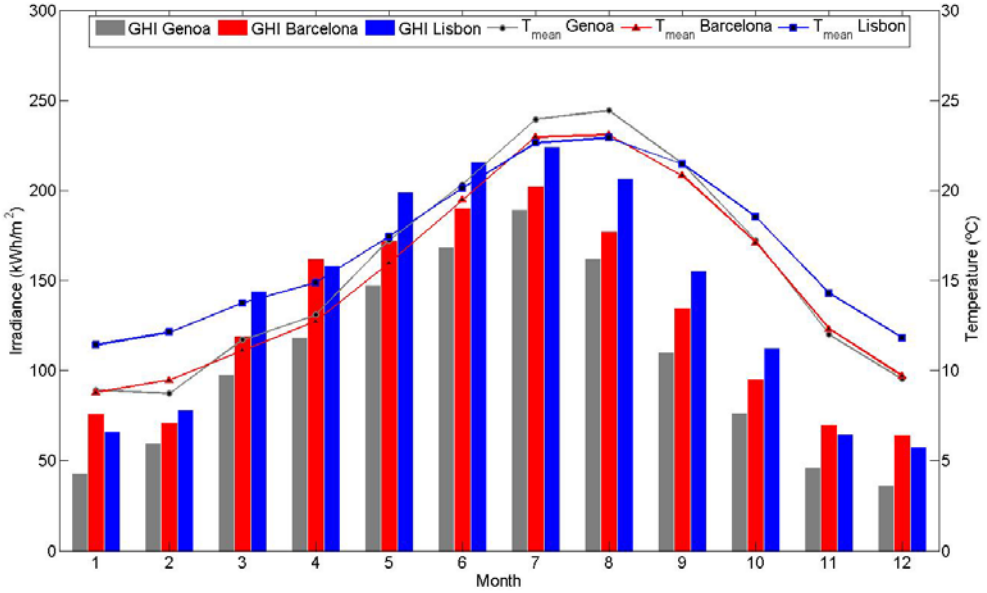

Figure 6. Monthly irradiances and mean temperatures for the selected cities.

3.2 Thermal and electrical demands

The energy demand considered corresponds to a standard four people family house. The heating season is considered to start on October, 16th and to finish on May, 15th and the cooling season from May,16th to October, 15th.

Heating and cooling demands (SH&C) have been determined using the TRNbuild tool and the building characteristics described in Subsection 2.2. The building envelope thermal characteristics considered are included in table 5. The internal heat gains generated by occupancy, lighting and appliances have been considered and calculated according to EN16798-1 standard [18].This norm also indicates the values for ventilation rates including infiltration, which for the present case takes a value of 42 l/sm^2 (residential building with normal level of expectation). The space heating and cooling demands are calculated to maintain an interior temperature of 20 ºC in winter and 26ºC in summer (latent control not applied). In summer, free cooling strategy by windows opening at night proposed by [19] has been adopted and, in consequence, cooling energy demand at night is reduced. Figure 7 describes the windows opening strategy that has been implemented, assuming a ventilation rate of 2 h^{-1}.

Two cases have been considered to evaluate the energy contribution of the proposed system. The first case, named as reference case, has been modeled without the CPVT system to fix the thermal energy demands originated by heating and cooling loads covered with a reversible heat pump and domestic hot water (DHW) delivered by a gas boiler. The second case comprises the building with the equipment of the reference case but with the CPVT superimposed. The heating load is covered by the same heat pump as in the first case but aided by a radiant floor (RF). The heat pump electricity need is partly covered by the CPVT electric generation and the RF is fed with the CPVT heat production. DHW

is also partly covered by the CPVT thermal energy production. In regard of electrical demands due to appliances and lighting, both cases considered the same items. In the reference case covered by grid connection and in the second one partly by the CPVT electricity generation.

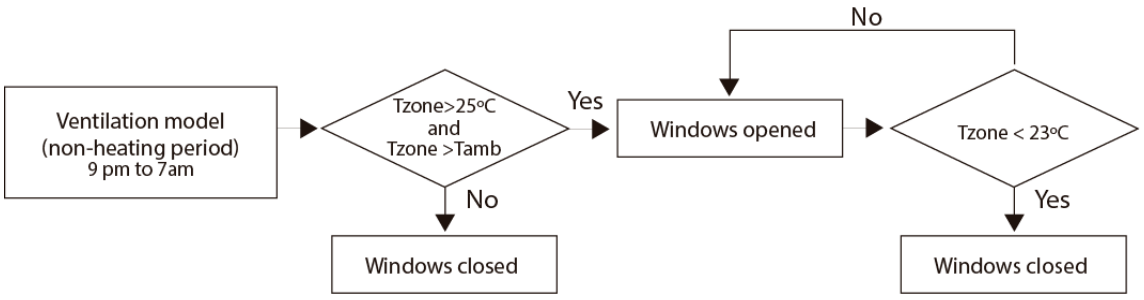

Figure 7. Strategy of windows opening for free cooling at night

Table 5. Envelope thermal characteristics

Elements	**U-value** (W/m^2K)	**g-value**
Walls	0.5	-
Roof	0.47	-
Ground Floor	0.53	-
Windows	2.5	0.7

The domestic hot water (DHW) demand has been determined following EN 15316-3-1 [20] and assuming the same water consumption for all cities: 26.5 liters per person at 60 ºC. The consumption profile has been calculated using the software DHWcalc [21]. A correction has been introduced assuming the service temperature is set to 45ºC instead of 60ºC as follows:

$$\dot{m}' = \frac{\dot{m}_{DHWcalc} \cdot (60 - T_{main\ water})}{(45 - T_{main\ water})} \quad (1)$$

The mass flow rate obtained by DHWcalc for rising the water from the main water circuit temperature ($T_{main\ water}$) to 60 ºC is increased by the factor described in Eq.(1) to obtain the corrected mass flow ($\dot{m}'$).

The main parameters and assumptions adopted for the SH&C and DHW demands are summed up in Table 6.

Table 6. Assumptions

Description	Value	Units
Set point in heating period	20	°C
Set point in cooling period	26	°C
Set point DHW	45	°C
Occupation rate [18]	42.5	m^2/per.
Nº of people	4	-
Heat gains per person (sensible) [18]	80	W
Heat gains per person (latent) [18]	40	W
Ventilation including infiltration [18]	0.42	$l \cdot s^{-1} \cdot m^{-2}$
Light heat gains [18]	8	$W \cdot m^{-2}$
Appliances heat gain [18]	2.4	$W \cdot m^{-2}$
Hourly schedules of lighting [18] Occupancy schedule (h) [18] Hourly schedules of appliances [18]	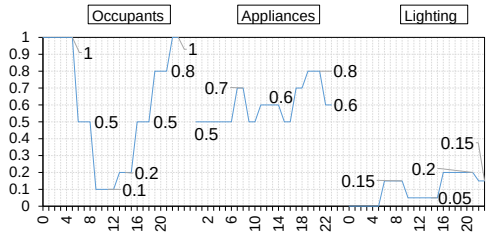	
Natural ventilation rate at night (summer period)	2	h^{-1}

The electrical energy demand profiles have been estimated considering the demands shown in Table 7 due to appliances and illumination points (A&L) resulting in an estimated electrical daily consumption of 5.45 kWh. The electrical consumption profile is adjusted so that the highest demands are between 11-15h and 18-23h. The heat pump electrical demand is derived from the thermal energy demand analysis.

Table 7. Estimated demands of light and appliances

Item	Power (W)	Daily usage (h)	Demand per day or cycle (Wh)
Combi fridge-freezer A+	175	12	2100
Dishwasher	300-1500	1.5	450
Microwave oven	1200	0.2	240
LCD TV	150	3	450
Washing machine	400-2500	1	475
Computer	150	3	450
Hairdryer	600	0.5	300
Other appliances	-	-	200
Lights	200	4	800

The SH&C, DHW and electrical annual demands obtained for the three locations considered are included in Table 8.

Table 8. Summary of annual energetic demands

Location	DHW (kWh/m^2)	SH (kWh/m^2)	SC (kWh/m^2)	Electricity (kWh/m^2)
Lisbon	16.3	53.3	12.6	31.7
Barcelona	16.9	74.4	11.1	37.5
Genoa	16.7	80.2	15.5	40.2

The DHW energy demands are very similar in the three selected locations. Regarding Space Heating (SH) demands, the demand in Genoa is 50.4% higher than in Lisbon due to its lower ambient temperatures and irradiances, whereas for Barcelona is very similar. The SC demand is the highest in Genoa followed by Lisbon. Finally, the electricity follows the same tendency than the SH demands. The high SC demand observed for Genoa, even to be counterintuitive, corresponds to the temperature profile registered for summer season, which is the highest of the three locations (Fig. 6).

3.3 Simulated system topology

The model presents three main parts that correspond to the thermal circuit (DHW and SH&C), electrical circuit and the building. The building has been modeled using TRNbuild, as indicated previously, to generate the energetic demands (see section 3.2). The general topology is depicted in Figure 8, including all the subsystems and its corresponding components.

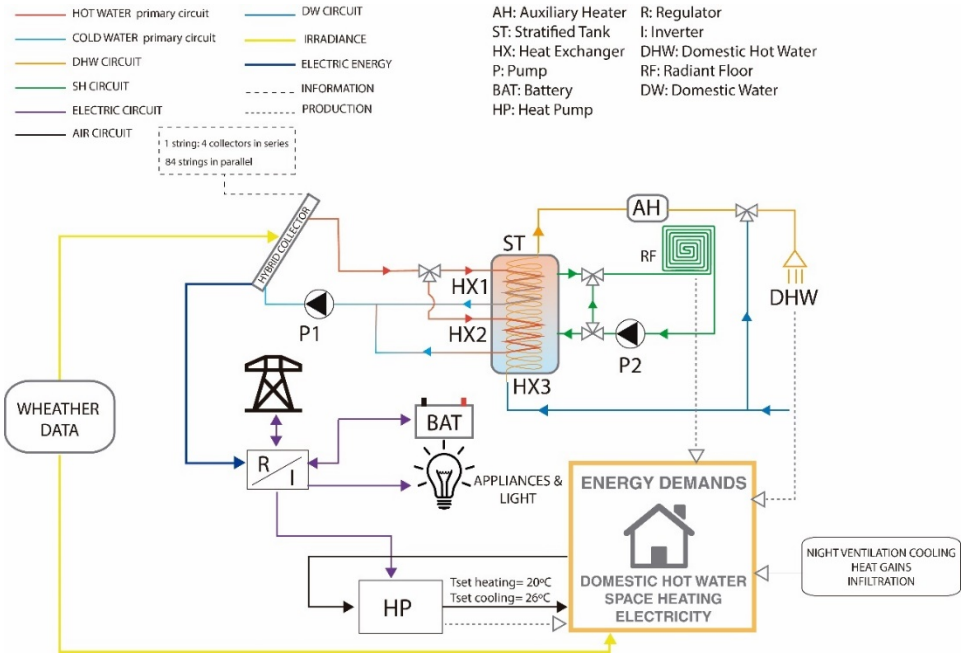

Figure 8. Simulated system topology

3.3.1 Thermal circuits

The solar thermal circuit is composed of the CPVT system, a pump (P1) and a stratified tank (ST) with three heat exchangers (HX1/2/3). The pump (P1) is controlled by a differential controller which compares the temperatures at the CPVT collector and at the lower part of the stratified tank (ST). The solar circuit works (P1 on) when the temperature difference exceeds the upper dead band (ΔT_{on}=6°C) and stays on until the temperature difference falls below the lower dead band (ΔT_{off}=2°C). Three heat exchangers are incorporated into the system, one (HX1) atop of the other (HX2) to achieve a better stratification and therefore a better efficiency from energy coming from solar collector. Hot water coming from the collector goes through HX1 or HX2 depending on its temperature. A differential controller compares the temperature of the solar collector with the temperatures at the inlet and at the outlet of the HX2. If the difference is greater than the upper dead band (ΔT_{on}) the fluid from the solar collector flows in HX1 whereas when this difference is lower than the lower dead band (ΔT_{off}), the HX2 is used. HX3 is used to provide DHW and the interior cavity is used to supply warm water to the radiant floor (RF). HX3 crosses the whole tank, thus achieving priority in front of the RF, which has its inlet from the tank below HX3 outlet and it is used for SH support.

There is also an auxiliary heater (AH), gas condensation burner, to provide DHW when the temperature at the outlet of HX3 is lower than 45ºC. The RF system works in parallel with the heat pump as long as there is heating demand and the impulsion flow temperature is higher than 25ºC. Regarding the RF, two valves allow controlling that the impulsion temperature does not exceed 42ºC and that the installation works until the return temperature achieved becomes lower than 25ºC.

3.3.2 Electrical circuit

The electrical energy produced by the CPVT system serves to partially cover demands of electrical A&L and the heat pump (for SH&C). If the electrical demand is lower than the production, batteries are charged to increase the degree of self-consumption for periods of higher demands. The conventional electric system remains in the building as an auxiliary system.

The operating mode adopted is the so-called “self-consuming connected to public power grid with backup batteries”. This mode allows working in parallel with the grid but always prioritizing the energy supplied by the PV system. Energy supplied by the PV system (direct current) is stored into the battery with the regulator and it is converted into alternating current by an inverter. If there is no demand and the batteries are fully charged, the surplus goes into the public power grid.

3.3.3 TRNSYS components

Different components have been included in TRNSYS in order to model this topology (Figure 8) such as pumps, valves, tanks, heat pump, pipes (losses), controllers, etc. In addition, to consider the energetic contribution to the building of the radiant floor an active layer has been created through the interface TRNbuild (Type56). Table 9 contains all the TRNSYS types used in the model, jointly with their main characteristic parameters.

Nevertheless, the concentrating PVT system considered in this study is not available in the TRNSYS library. There are types for standard PVT systems such as types 50 or 563, however, those types are not designed to have cells directly immersed on dielectric liquids and under concentrated irradiance conditions. Therefore, a new type has been developed to model the present CPTV collector. The type includes the wind speed dependence on the steady-state thermal characteristic and the electrical model temperature dependence. The main equations that govern the model are shown below. Figure 9 depicts the flow chart of the new type.

The thermal efficiency has been implemented, based on the Hottel-Whillier model [22], as:

$$\eta_T = \frac{\dot{q_u}}{I_T} = \frac{\dot{m}\ C_p\ (T_o - T_i)}{A\ I_T} = F_R(\tau\alpha)_n - F_R\ U_L \frac{(\Delta T_m)}{I_T} \tag{2}$$

$$\dot{q_u} = F_R(\tau\alpha)_n \cdot I_T - F_R\ U_L\ (\Delta T_m) \tag{3}$$

With $(\Delta T_m) = T_m - T_{amb}$, $T_m = \frac{1}{2}(T_{in} + T_{out})$ and where $\dot{q_u}$ is the heat output of the collector per area (W/m^2), F_R is the collector heat removal factor, U_L is the overall heat loss coefficient and $(\tau\alpha)_n$ is the effective transmittance-absorptance product. The wind dependence is incorporated to the model by applying two correction terms into Eq.(3). The first term corrects the effect on the zero loss coefficient ($-c_{w0}\ u_w \cdot I_w$) and the another accounts for the wind influence on heat losses ($-c_{w1}\ u_w \cdot \Delta T_m$). The useful modified output can be written as:

$$\dot{q_u} = F_R(\tau\alpha)_n \cdot I_T - c_{w0}u_w I_T - F_R\ U_L\ (\Delta T_m) - c_{w1}u_w\ (\Delta T_m) \tag{4}$$

The first part of the equation describes the radiative balance of the collector, which is independent of the collector temperature. These two terms are named as $\dot{q}_{rad}$:

$$\dot{q}_{rad} = F_R(\tau\alpha)_n \cdot I_T - c_{w0}u_w I_T \tag{5}$$

The heat gain and the collector output are calculated by means of an iterative process. First, the heat gain is calculated:

$$\dot{q}_u\ = \left(\dot{q}_{rad} - F_R\ U_L\ (\Delta T_m) - c_{w1}u_w\ (\Delta T_m)\right) \tag{6}$$

Then, the outlet temperature T_{out} of the current time step is calculated from the collector heat gain with the T_{out} from the previous time step and the collector and flow parameters of the current time step:

$$T_{out} = T_{in} + \frac{\dot{q}_u}{\dot{m} \cdot C_p} \tag{7}$$

In the case that there is no mass flow:

$$T_{out} = T_{amb} + I_t \cdot (F_R(\tau\alpha)_n - c_{w0})/(F_R\, U_L + c_{w1}) \quad (8)$$

The electric power at maximum power point (P'_{mpp}) supplied by the solar collector has been programmed to be coupled with the thermal part by the cell temperature. The cell temperature, T_c, is calculated with Eq. (9) as a function of the fluid inlet temperature T_i, the collector thermal efficiency η_T and the incident irradiance G [23].

$$T_c = T_i + \left(\frac{1 - F_R}{F_R\, U_L}\right)\eta_T \cdot G \quad (9)$$

As a consequence, the solar electric power for cell temperatures different from the standard conditions one (P'_{mpp}) can be obtained by Eq. (10) [24].

$$P_{mpp} = C_g \cdot \eta_{opt} \cdot \frac{G}{G_{STC}} I_{SC,STC} \cdot V_{OC} \cdot FF$$
$$P'_{mpp} = P_{mpp}\left[1 + \gamma\left(T_c - T_{c,STC}\right)\right] \quad (10)$$

Where subscript STC indicates that parameters are referred to standard test conditions (STC). This means a **cell temperature of 25°C** and an **irradiance of 1000 W/m^2.**

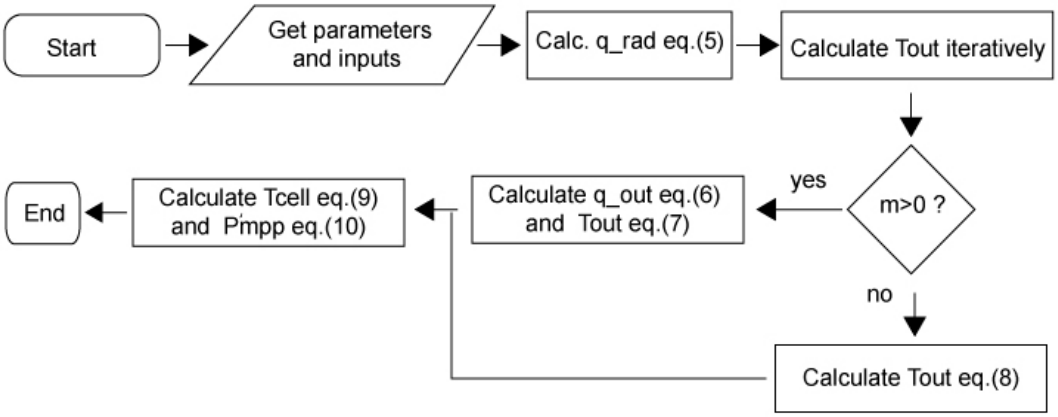

Figure 9. Flow chart of the new type.

Table 9. Parameters of principal components used in TRNSYS model

Parameter	Description	Value	Units
Battery	Type 47a		
Battery tech.	Li-ion		
Model	LG- Resu 10 ([25]		
$C_{battery}$	Battery capacity	10	kWh
Inverter/Regulator	Type 48b		
$\eta_{regulator}$	Regulator efficiency	0.9	-
$\eta_{inversor}$	Inverter efficiency	0.9	-
$P_{inverter}$	Power of inverter	4.5	kW
Auxiliar Boiler	Type 6		
Model	Bosch ZBR 16-3 [26]		
P_{boiler}	Maximum power of boiler	16.7	kW
η_{boiler}	Efficiency of boiler	0.9	-
$T_{set\ DHW}$	DHW set point	45	°C
Heat Pump	Type 665 (1 unit per zone)		
Model	Mitsubishi PUHZ-ZRP50VKA [27]		
$P_{heat/cool}$	Rated heating / cooling power per zone	6/5	kW
COP	Nominal coefficient of performance (Heating)	4	-
EER	Nominal energy efficiency ratio (Cooling)	3.5	-
Tank	Type 534		
C_{tank}	Capacity	2	m^3
H_{tank}	Height	2.16	m
TL_{tank}	Thermal losses	1.18	kJ/m^2k
nHX	Nº heat exchangers	3	-
Radiant floor	Active layer, type 56		
D_{pipe}	Diameter of pipe	0.02	m
S_{pipe}	Space between center to center pipe	0.2	m
T_{pipe}	Wall thickness of pipe	0.002	m
K_{pipe}	Conductivity wall of pipe	0.35	W/m^2K
$\dot{m}_{RF}$	Flow rate of radiant floor	1200	kg/h

4. Results

Regarding the thermal energy production of the CPVT system, the priority is to satisfy DHW demand prior to SH demand by means of the radiant floor. The solar fraction has been calculated in order to evaluate the percentage of DHW covered by the system. The solar fraction is the share of the total conventional domestic hot water heating demand (consumption and tank standby losses) which is covered by the CPVT system. The higher the solar fraction, the greater the solar contribution to water heating, which reduces the energy required by the auxiliary water heater (gas burner). It is defined as:

$$SF_{DHW} = 100\left(1 - \frac{Energy\ DHW, auxiliary}{Energy\ demand\ DHW}\right) \quad (11)$$

The DHW demand, DHW solar production and the solar fraction can be seen in Figure 10a for the three selected cities. The DHW demand is well covered in Lisbon and Barcelona achieving an annual solar fraction above 75% (77.5% in Lisbon and 76.6% in Barcelona). Lisbon presents the minimum SF in December with 51.3% and Barcelona in February with 55.4%. Both cities achieve higher SFs during summer due to the higher irradiances. In the case of Genoa, the annual solar fraction obtained is 61.2%, slightly lower than in the previous locations. The temperatures in Genoa are rather similar to those in Barcelona, however, the incident irradiance is lower and consequently the solar production decreases. This results in lower SFs especially during the winter period when the ambient temperatures and irradiances are low. Nonetheless, the SF is still within reasonable values. The annual solar productions for DHW in Lisbon, Barcelona and Genoa are 1822.99 kWh, 1869.76 kWh, and 1477.47 kWh respectively.

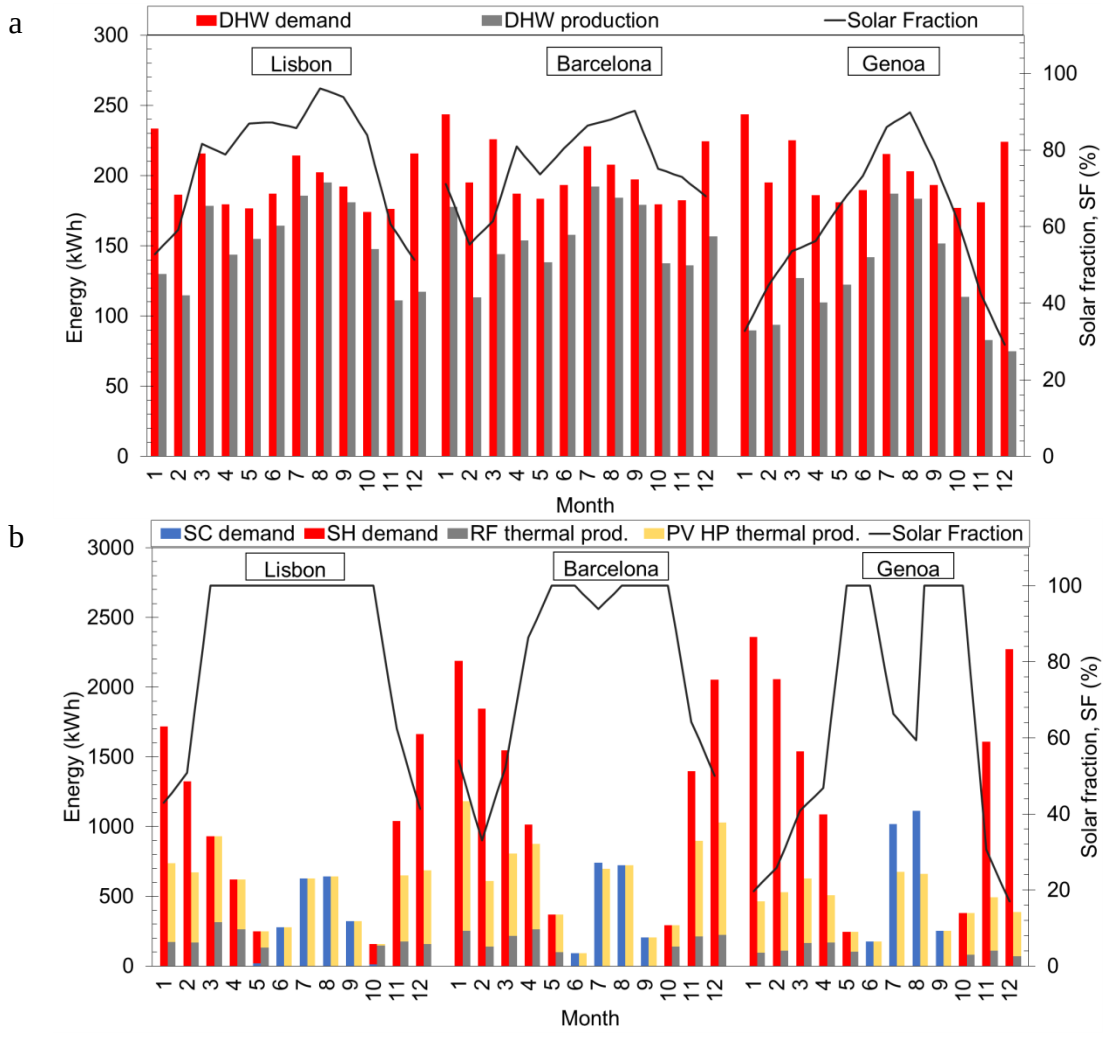

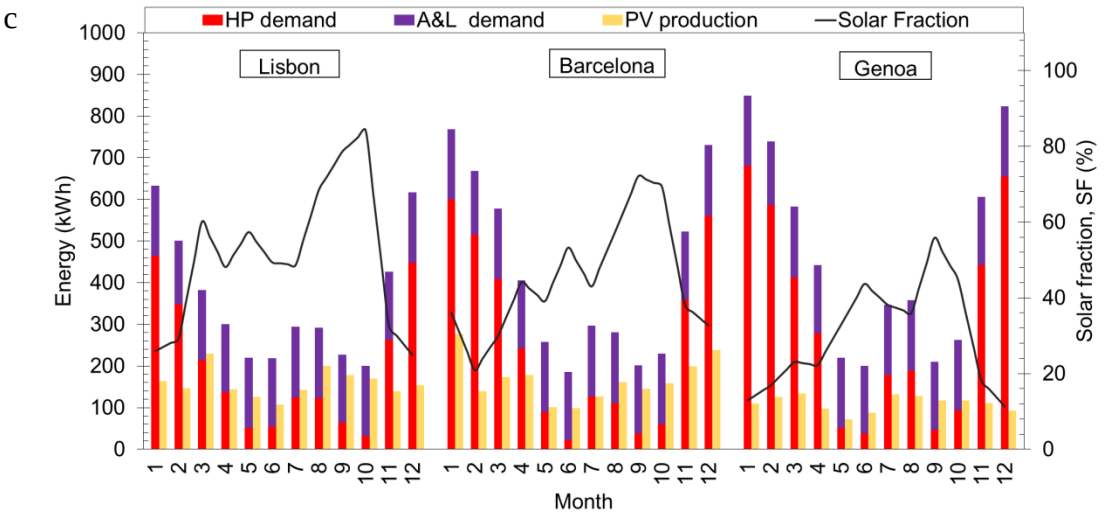

Figure 10. Energy demands, productions and solar fractions for Lisbon, Barcelona and Genoa. (a) DHW, (b) SH&C demands, radiant floor (RF) and pump (HP) powered by PV modules thermal productions (c) electricity.

The CPVT system also aims at partially covering the SH&C demands by means of a radiant floor (RF) (only for SH) and by powering the heat pump (HP) with the electrical energy produced by the PV modules (SH&C).

In an analogous manner, the solar fraction covering the SH&C demand is expressed as the quotient of the thermal energy needed with the HP connected to the grid and the energy demand:

$$SF_{SH\&C} = 100\left(1 - \frac{Energy\ SH\&C\ from\ grid}{Energy\ demand\ SH\&C}\right) \quad (12)$$

Finally, the electrical solar fraction is obtained rating the electrical energy yielded by the CPVT module with the electrical energy demand.

$$SF_{ELECTRIC} = 100\left(\frac{Electrical\ energy\ from\ CPVT}{Electric\ energy\ demand}\right) \quad (12)$$

Figure 10b shows the SH&C demands together with the RF thermal production, the thermal production by the HP powered with the PVs and the associated SF. The three selected cities show similar trends in the SF with high values close to 100% during summer and production mean percentages ranging from 20 to 50 % during winter. The CPVT system is able to cover all the demands in Lisbon during summer due to its moderate SC demand. Barcelona achieves also a high solar fraction in summer, however, the system is not able to cope with SC demand in July. Genoa has the highest SC demand during July and August and therefore the system can only achieve a SF slightly higher than 60%.

During winter Barcelona and Lisbon can only be covered with around 50% of the SH demands whereas in Genoa due to the previously mentioned lower irradiance and temperature values, the collector is less efficient and a fraction of around 30% is attained.

The mean annual SFs achieved are: 68.7% for Lisbon, 62.4% for Barcelona and 38.3% for Genoa.

Finally, the electrical results are plotted in Fig. 10c. Electrical demands are differentiated between A&L and the electricity needed for the HP. SFs result in lower values than those stated for DHW and SH&C: Lisbon = 44.09%, Barcelona = 38.9% and Genoa = 23.51%. The difference respect SF values for SH&C is due to the effect of the A&L, since the HP either considered as thermal or electrical item by means of the COP and the EER has the same SF.

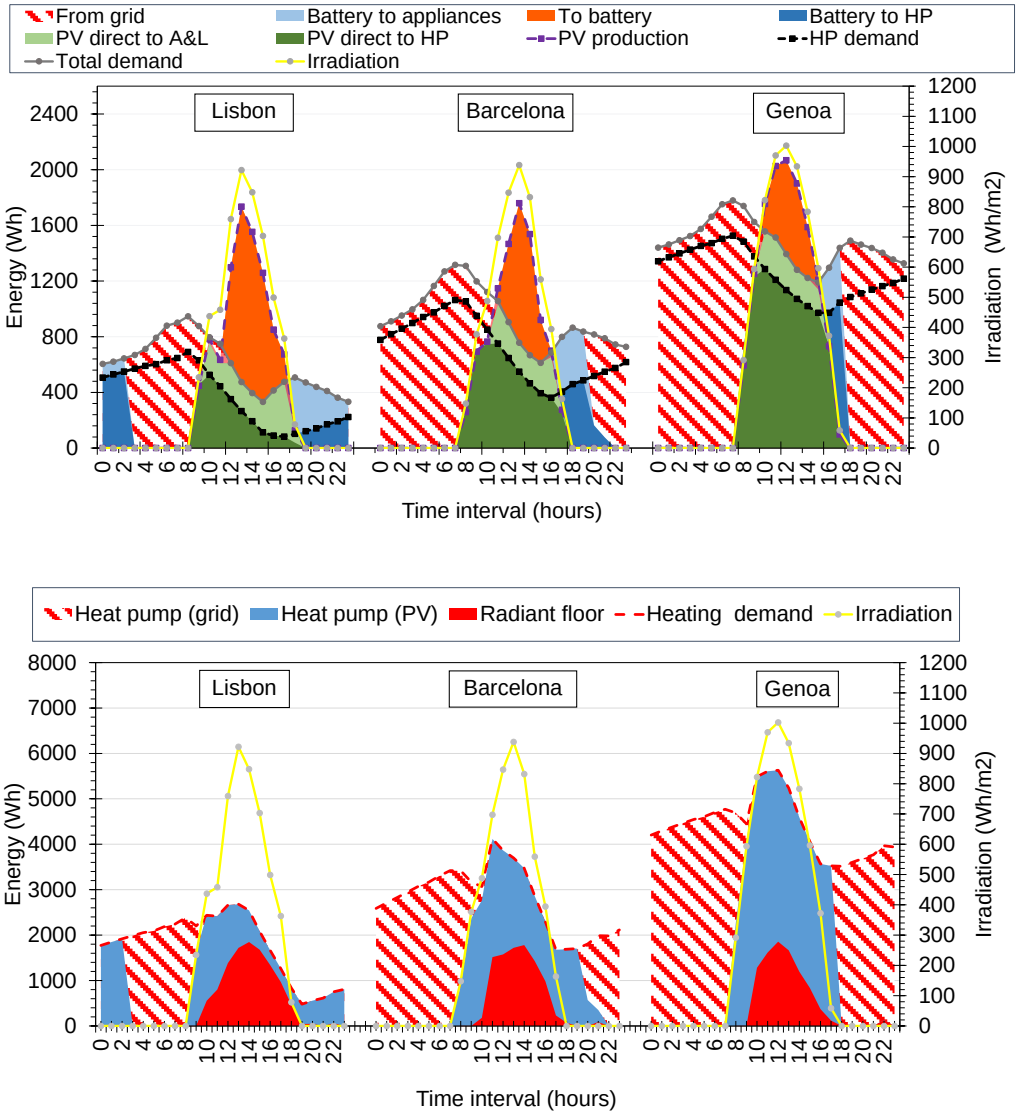

Figure 11. Daily electrical (top) and thermal (bottom) profiles for a typical winter day and for the three locations.

Figure 11 plots the detailed daily profiles of a winter day for the electrical and space heating and cooling loads jointly with how these loads are covered. Also the irradiation is included to better appreciate the periods where direct consumption from the CPVT installation is possible or the energy is obtained either from the battery or the grid. In

regard of the electrical demand (Fig. 11 top), the demand is differentiated between appliances plus lighting and heat pump. In addition, it can be distinguished the fraction of the electrical production that charges the battery. For instance, in the case of Lisbon the day starts taking energy from the battery charged the previous day. Once the battery is over, the electricity is obtained from the grid. At the moment when the sun rises, the heat pump and the appliances and lighting are directly fed by the CPVT collector. The energy exceeding the demand is utilized to charge the battery. When irradiation decreases, part of the demand is progressively covered by the battery till the sunset onwards, where the battery satisfies 100% of the demand. On the other hand, the space heating demand and production is explained in Fig 11 bottom. It can be appreciated the periods where the demand is partly covered by the radiant floor and concerning the rest of the demand the fraction that is covered by the heat pump either with electricity produced by the CPVT (direc consimption or battery) or plugged to the grid.

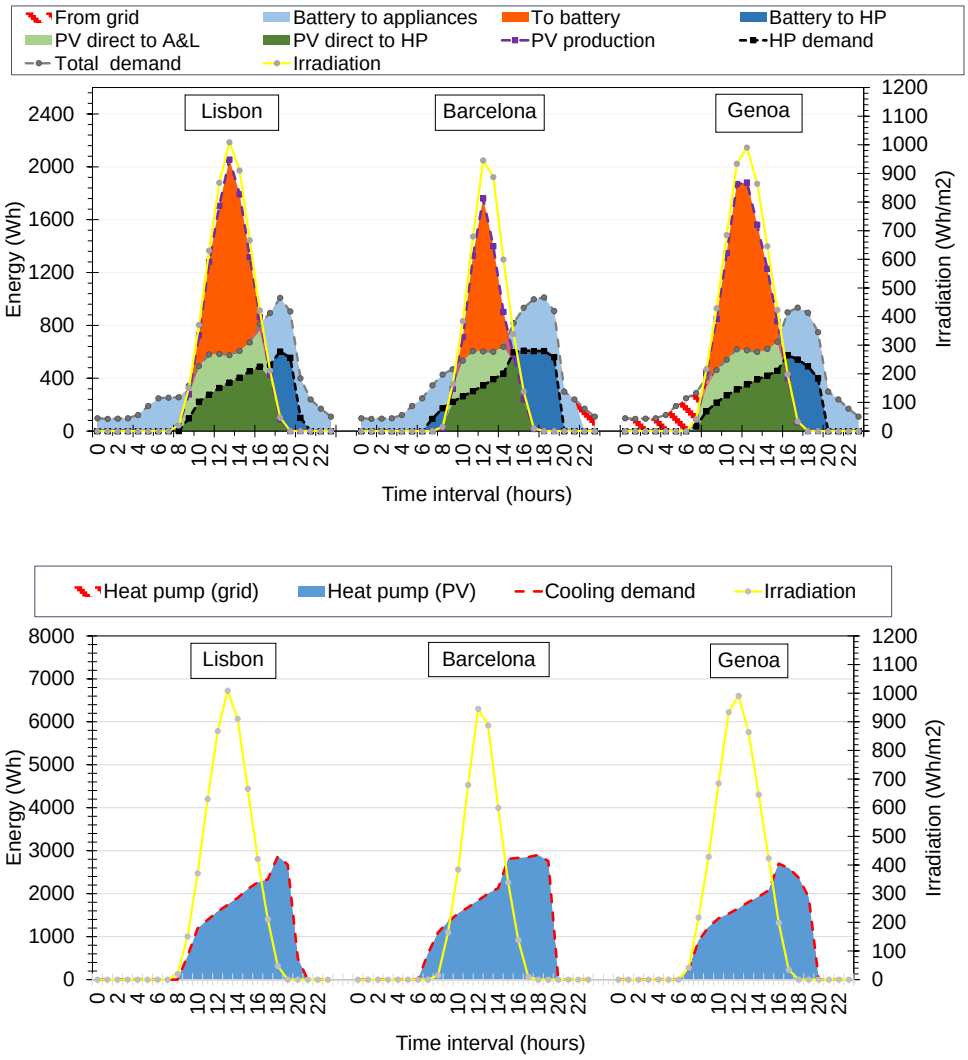

Figure 12. Daily electrical (top) and thermal (bottom) profiles for a typical summer day and for the three locations.

Figure 12 describes the electrical and SH&C profiles for a typical summer day and for the three locations. It can be seen that in all the cities the system production almost satisfies the demands totally. Very short time periods need electricity from the grid to

cover the appliances and lighting demand for the case of Barcelona and Genoa, whereas in the case of Lisbon there is no need of grid connection.

Based on the obtained results for the three simulated cities, it can be deduced that the performance of the CPVT collector analyzed is satisfactory for all the cases but in the case of Genoa the thermal performance is in the limit of achieving satisfactory solar fraction values. As indicated in Section 3.1, the limitations of the CPVT collector (high heat loss coefficient and shading for low latitudes achieving high solar altitudes) indicate system suitability for locations with mild winters and latitudes with not so high solar heights (i.e. not above 75º). This fact has been proven by the results obtained that demonstrate the appropriateness of the system for three selected cities with mild winters and hot summers representative of Csa climate and latitudes in the interval 38.7 º (Lisbon) - 44.4 º (Genoa), which means maximum solar altitudes for the case of Lisbon of around 74º.

5. Conclusions

A building-integrated concentrating photovoltaic-thermal (CPVT) system with direct immersion of solar cells has been modeled and simulated with TRNSYS 16 in three different cities representative of mild winter and hot summer climate: Lisbon, Barcelona and Genoa. A new TRNSYS type has been programmed based on the CPVT module performance assessment. Specifically, the thermal performance of the collector has been analyzed numerically and experimentally in the frame of the present research.

The concentrating system, which tracks the solar height and acts as a shading controller, has been placed in front of the windows of the south facing façade on a two-story four-person single-family house.

The thermal energy generated by the CPVT system aims to cover the domestic hot water demand, which is the priority, and partially the space heating energy requirements by means of a radiant floor. In addition, the electrical energy generated by the PV cells is designed to cover the electrical demands of lighting and appliances and to power an air-air reversible heat pump for space heating and cooling.

Regarding the domestic hot water energy demands, the annual average solar fractions (SFs) found are higher than 74.0% in Lisbon and Barcelona and 52.6% in Genoa. In addition, the potential of the CPVT system could provide SFs for space heating and cooling of 68.7% in Lisbon, 62.4% in Barcelona and 38.3% in Genoa. Finally, in the case of electrical loads, SFs take a value of 44.09% in the case of Lisbon, 38.9% for Barcelona and 23.51% for Genoa.

The performance of the CPVT collector analyzed is satisfactory for all the cases but in the case of Genoa the thermal performance is in the limit of achieving satisfactory solar fraction values. The limitations of the CPVT collector (high heat loss coefficient and shading for low latitudes achieving high solar altitudes) indicate system suitability for locations with mild winters and latitudes with not so high solar heights (i.e. not above 75º). This fact has been proven by the results obtained that demonstrate the appropriateness of the system for three selected cities with mild winters and hot summers representative of Csa climate and latitudes in the interval 38.7 º (Lisbon) - 44.4 º (Genoa), which means maximum solar altitudes for the case of Lisbon of around 74º.

Acknowledgements

The authors would like to thank "Ministerio de Economía y Competitividad" of Spain for the funding (grant references ENE2013-48325-R, ENE2016-81040-R and BES-2014-069596) and “Generalitat de Catalunya” for the grant 2017FI_B_01171.

References

1. EPBD, *Energy Performance of Buildings (EPBD) Directive 2010/31/EU* (European Parliament, 2010).
2. A. H. A. Al-Waeli, K. Sopian, H. A. Kazem, and M. T. Chaichan, "Photovoltaic/Thermal (PV/T) systems: Status and future prospects," Renew. Sustain. Energy Rev. **77**, 109–130 (2017).
3. R. M. da Silva and J. L. M. Fernandes, "Hybrid photovoltaic/thermal (PV/T) solar systems simulation with Simulink/Matlab," Sol. Energy **84**, 1985–1996 (2010).
4. D. Chemisana, "Building Integrated Concentrating Photovoltaics: A review," Renew. Sustain. Energy Rev. **15**, 603–611 (2011).
5. C. Lamnatou and D. Chemisana, "Concentrating solar systems: Life Cycle Assessment (LCA) and environmental issues," Renew. Sustain. Energy Rev. **78**, 916–932 (2017).
6. C. Lamnatou and D. Chemisana, "Photovoltaic/thermal (PVT) systems: A review with emphasis on environmental issues," Renew. Energy **105**, 270–287 (2017).
7. Y. A. Abrahamyan, V. I. Serago, V. M. Aroutiounian, I. D. Anisimova, V. I. Stafeev, G. G. Karamian, G. A. Martoyan, and A. A. Mouradyan, "The efficiency of solar cells immersed in liquid dielectrics," Sol. Energy Mater. Sol. Cells **73**, 367–375 (2002).
8. Y. Sun, Y. Wang, L. Zhu, B. Yin, H. Xiang, and Q. Huang, "Direct liquid-immersion cooling of concentrator silicon solar cells in a linear concentrating photovoltaic receiver," Energy **65**, 264–271 (2014).
9. D. Chemisana, E. F. Fernandez, A. Riverola, and A. Moreno, "Fluid-based spectrally selective filters for direct immersed PVT solar systems in building applications," Renew. Energy (2018).
10. X. Ju, C. Xu, X. Han, X. Du, G. Wei, and Y. Yang, "A review of the concentrated photovoltaic/thermal (CPVT) hybrid solar systems based on the spectral beam splitting technology," Appl. Energy **187**, 534–563 (2017).
11. X. Han, Y. Wang, and L. Zhu, "Electrical and thermal performance of silicon concentrator solar cells immersed in dielectric liquids," Appl. Energy **88**, 4481–4489 (2011).
12. R. Looser, M. Vivar, and V. Everett, "Spectral characterisation and long-term performance analysis of various commercial Heat Transfer Fluids (HTF) as Direct-Absorption Filters for CPV-T beam-splitting applications," Appl. Energy **113**, 1496–1511 (2014).
13. M. Vivar and V. Everett, "A review of optical and thermal transfer fluids used for

optical adaptation or beam-splitting in concentrating solar systems," Prog. Photovoltaics Res. Appl. **22**, 612–633 (2014).

14. SAS Silicon cells, "SR6SKUN 156.75 x 156.75 Monocrystalline Solar Cell 5 Bus bars," (2017).
15. S. W. Churchill and M. Bernstein, "A Correlating Equation for Forced Convection From Gases and Liquids to a Circular Cylinder in Crossflow," J. Heat Transfer **99**, 300 (1977).
16. S. Klein and W. Beckman, "TRNSYS 16: A transient system simulation program: mathematical reference," (2004).
17. M. Kottek, J. Grieser, C. Beck, B. Rudolf, and F. Rubel, "World Map of the Köppen-Geiger climate classification updated," eschweizerbartxxx Meteorol. Zeitschrift **15**, 259–263 (2006).
18. CEN, "prEN 16798-1: Energy performance of buildings - Part 1: Indoor environmental input parameters for design and assessment of energy performance of buildings addressing indoor air quality, thermal environment, lighting and acoustics - Module M1-6," **44**, (2015).
19. A. Buonomano, F. Calise, A. Palombo, and M. Vicidomini, "BIPVT systems for residential applications : An energy and economic analysis for European climates," Appl. Energy **184**, 1411–1431 (2016).
20. CEN, "EN 15316-3-1 - Heating systems in buildings - Method for calculation of system energy requirements and system efficiencies - Part 3-1: Domestic hot water systems, characterisation of needs," (2008).
21. U. Jordan and K. Vajen, "DHWcalc: PROGRAM TO GENERATE DOMESTIC HOT WATER PROFILES WITH STATISTICAL MEANS FOR USER DEFINED CONDITIONS," in *ISES Solar World Congress* (2005).
22. J. A. Duffie and W. A. Beckman, *Solar Engineering of Thermal Processes* (Wiley, 2013).
23. B. Sandnes and J. Rekstad, "A photovoltaic/thermal (PV/T) collector with a polymer absorber plate. Experimental study and analytical model," Sol. Energy **72**, 63–73 (2002).
24. D. L. Evans, "Simplified method for predicting photovoltaic array output," Sol. Energy **27**, 555–560 (1981).
25. LG CHEM, "ESS Battery," .
26. Bosch Thermotechnology, "Gas-Fired Wall Mounted Condensing Boilers," .
27. Mitsubishi Electric, "Technical documentation," .